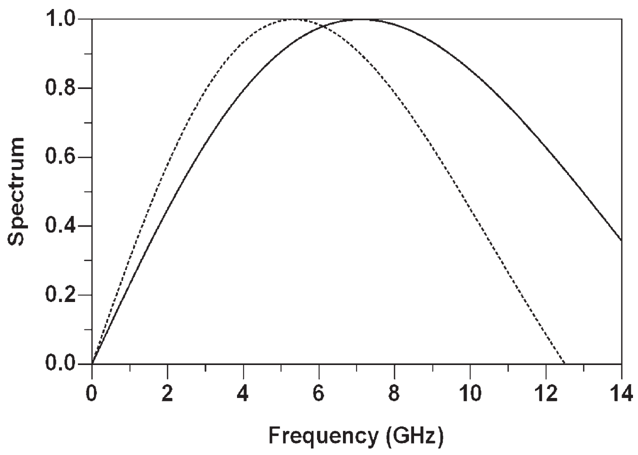

Figure 6 Normalized spectrum of the signal generated with two PCSs having different carrier lifetime

The delay time of the optical command and the pulses width can be chosen in our PCS electrical model. The pulses width has been selected from 1 to 140 ps. The first PCS has been biased at 1.5 V and the second one at −1.5 V. The peak value of the photogenerated pulses depends on photoconductivity through carrier lifetime. The pulses peak voltage varies between 10 and 164 mV for an average optical power of 60 mW.

Simulation results of this topology are represented in Figure 6 for a repetition time of 2 ns corresponding to the parameters of the previous source laser. The energy of this signal is focused in the frequency band 3–12 GHz and can be shifted by pulses duration and the second impulse time delay. For these results, the delay time has been considered at the extremity of the first impulse. Then, the increase of the pulses FWHM by adjusting carrier lifetime induces the reduction of spectrum bandwidth. The dashed curve is obtained for total monocycle impulse duration of 160 ps and the continued curve for a total time of 130 ps. Such electrical pulses can be generated with PCS on LT-GaAs substrate with carrier lifetime of 10th picosecond. The photogenerated pulses bandwidth at −10 dB is higher than the required FCC emission limit. To delete the unwanted extremity band power, an emission antenna is used as a specific filter.

5. CONCLUSIONS

A UWB signal generation method exploiting a photoconductive effect on GaAs semiconductor is presented. The base device consists of a transmission line discontinuity where illuminated by optical pulsed command induces electrical pulses generation. Measurement results of TX/RX system with a PCS on LT-GaAs and GaAs substrates have been shown the ability of a broadband signal generation by optical pulses. A UWB antenna on alumina substrate has been first designed for this demonstration and will be optimized for the future system integration. The combination of positive and negative pulses demonstrates the generation ability of UWB signal. The same optical pulsed command is applied on the PCSs with an appropriate delay. For the emission bloc, the integrated antenna is used as a filter to select the radiated power to comply with FCC emission limit mask.

REFERENCES

1. Revision of part 15 of the Commission's Rules Regarding Ultra Wideband Transmission System, ET Docket 98-153, FCC, Washington, DC, February 14, 2002.
2. M. Abtahi, J. Magne, M. Mirshafiei, L.A. Rusch, and S. Laochelle, Generation of power-efficient FCC-compliant UWB waveforms using FBGs: Analysis and experiment, J Lightwave Technol 26 (2008), 628–635.
3. J. Yao and F. Zeng, Photonic generation of ultra wideband signals, J Lightwave Technol 25 (2007), 3219–3235.
4. S. Faci, C. Tripon-Canseliet, G. Alquie, S. Formont, and J. Chazelas, OOK modulator using photoconductive feedback oscillator, Microw Opt Technol Lett 52 (2010), 2010–2016.
5. C. Tripon-Canseliet, S. Faci, G. Alquie, K. Blary, S. Formont, and J. Chazelas, Magnitude modulation of microwave signals by ultrafast control of membrane LT- GaAs, J. Eur Microw Assoc 4 (2008), 244–250.
6. X. Liu, A. Prasad, W.M. Chen, A. Kurpiewski, A. Stoschek, Z. Liliental-Weber, and E.R. Weber, Mechanism responsible for the semi-insulating properties of low-temperature-grown GaAs, Appl Phys Lett 65 (1994), 3002–3004.
7. N. Guldner, C. Tripon-Canseliet, S. Faci, G. Alquie, Optically controlled UWB emission system, European Microwave Week, Rome, 2009.
8. W. Sörgel and W. Wiesbeck, Influence of the antennas on the ultra wideband transmission, EURASIP J Appl Signal Process (2005), 296–305.

NUMERICAL STUDY OF SINGULARITY EXTRACTION IN MoM INTEGRALS FOR SCATTERING FROM BODIES OF REVOLUTION

Úrsula C. Resende,[1] Fernando J. S. Moreira,[2] and Odilon M. C. Pereira-Filho[3]
[1] Department of Electrical Engineering, Federal Center of Technological Education of Minas Gerais, Belo Horizonte, MG 35510-000, Brazil; Corresponding author: resendeursula@des.cefetmg.br
[2] Department of Electronics Engineering, Federal University of Minas Gerais, Belo Horizonte, MG 31270-901, Brazil
[3] Center of Informatics, Federal University of Pernambuco, Recife, PE 50740-560, Brazil

Received 30 January 2012

ABSTRACT: *The analysis of electromagnetic scattering by the method of moments (MoM) leads to integral equations with singularities in their kernels. In this work, a numerical study of a particular technique for the extraction of those singularities arising in the analysis of the scattering from conducting and dielectric bodies of revolution (BOR), particularly spheres and cylinders is conducted. It is demonstrated that when the singularity extraction is applied, the numerical solution converges for a two-point Gaussian quadrature. It is also shown that the MoM matrix condition number is affected by the number of segments used to describe the BOR generatrix and this influence depends on the behavior of the surface current distribution.* © 2012 Wiley Periodicals, Inc. Microwave Opt Technol Lett 54:2543–2548, 2012; View this article online at wileyonlinelibrary.com. DOI 10.1002/mop.27160

Key words: *method of moments; electric and magnetic field integral equations; integral singularities; condition number and bodies of revolution*

1. INTRODUCTION

The numerical simulation of electromagnetic scattering from homogeneous and composite bodies has been thoroughly investigated due to its application in different areas of engineering. For bodies of revolution (BOR), the problem is reduced to a two-dimensional one, resulting in significant savings of computation time and memory storage. Conducting and composite BORs have been investigated in Refs. 1–4, where surface integral equations are numerically evaluated by the method of moments (MoM). However, the integrals involved are often singular and require special considerations for their numerical evaluation. These singularities occur in the kernels of self-terms, where testing and source subdomains coincide [1].

In this context, the choice of suitable basis functions to represent the equivalent surface current distribution, the numerical evaluation of singular integrals, and efficient algorithms for the linear-system solution are fundamental to obtain accuracy and convergence from the MoM analysis. However, the numerical evaluation of singularities arising in the integral kernels is not a simple task. In Ref. 5, the authors used the FFT technique to enhance the computational efficiency of the MoM analysis. Werner [6] derived an exact integration procedure for thin circular loop antennas and used the same procedure to analyze a moderately thick cylindrical wire antenna [7]. In Refs. 1 and 8, robust singularity extraction techniques were presented for the analysis of conducting BORs. In Refs. 9 and 10, the singularity extraction presented in Ref. 1 was extended to handle triangular basis functions (TBFs) in a Galerkin scheme for the solution of combinations of electric and magnetic field integral equations.

In the analysis of dielectric bodies, generally, the accuracy of the MoM simulations deteriorates as the relative permittivity increases. This problem can be partially overcome by increasing the number of segments used to represent the BOR generatrix, which should be made proportional to the dielectric constant. In Ref. 11, triangular functions for both basis and testing functions were used, represented by a series of pulses. It was observed that, to attain certain accuracy, more pulses had to be used to represent the triangular functions as the dielectric constant of the BOR was increased. In some sense, this may lead to the perception that accuracy increases with the number of quadrature points used to evaluate the integrals.

In this work, a numerical study of a MoM implementation is conducted with and without applying the singularity extraction of Refs. 9 and 10. TBFs, defined over two consecutive segments of a BOR generatrix, are used to represent the equivalent surface currents in $\hat{t}$ (along the BOR generatix) and $\hat{\phi}$ directions together with a Galerkin technique. From the results, it is observed that when the singularity extraction is applied the numerical convergence is attained with a two-point Gaussian quadrature. Accuracy increases when more TBFs are used. It is also verified that the MoM matrix condition number diminishes when the extraction technique is applied and it is significantly affected by the behavior of the equivalent current. For current distributions with small oscillations, the condition number increases significantly when more segments are used to represent the BOR generatrix. For highly oscillatory currents, the increase is less significant.

2. INTEGRAL EQUATION EVALUATION

In the MoM analysis of electromagnetic scattering, electric (EFIE) and magnetic (MFIE) field integral equations can be combined in many different ways [2–4]. The EFIE formulation is the usual choice for open conducting shells [2]. For closed conducting surfaces, the combined field integral equation (CFIE), which is a linear combination of EFIE and MFIE, avoids spurious resonances [2]. For dielectric bodies, EFIE and MFIE can be linearly combined in several forms, where Müller and PMCHW formulations are generally used for homogeneous dielectric bodies [3]. For BORs, these formulations with the following equivalent surface current representation

$$X(r') = \sum_{n=-\infty}^{\infty} \left[\sum_{j=1}^{Nt} I_{jn}^{Xt} \frac{T_j^t(t')}{\rho'} \, \hat{t}' + \sum_{j=1}^{N\varphi} I_{jn}^{X\varphi} \frac{T_j^{\varphi}(t')}{\rho'} \, , \hat{\varphi}' \right] e^{-jn\varphi'}, \quad (1)$$

lead to integrals of the form [9]:

$$I = \int_{\phi=0}^{2\pi} \int_{\alpha=-1}^{1} \int_{\alpha'=-1}^{1} \left(\frac{ab}{c} \right) F(\phi) \frac{e^{-jkR}}{R^d} d\alpha' \, d\alpha \, d\phi, \qquad (2)$$

where **X** represents either electric (**J**) or magnetic (**M**) equivalent currents, $T_j^t(t')$ and $T_j^{\phi}(t')$ are the TBFs, Nt and $N\phi$ are the number of TBFs, I_{jn}^{Xt} and $I_{jn}^{X\phi}$ are the unknown coefficients, the terms $e^{-jn\phi'}$ correspond to the Fourier expansion in ϕ, and the division by ρ' prevents singularity problems at the symmetry axis. In Eq. (2), $R = |\mathbf{r} - \mathbf{r}'|$ is the distance between source and observation points; a is equal to 1, α', or α'^2; b is equal to 1, α, or α^2, c is equal to 1, ρ, ρ', or $\rho\rho'$, and the exponent $d =$ 1 or 3. The coordinates t and t' measured along the BOR generatrix are parameterized in terms of α and α'.

The integral (2) cannot be analytically evaluated and has removable singularities whenever the observation (field) point $\mathbf{r}$ is very close to the source point $\mathbf{r}'$. The concept adopted in Refs. 1 and 9 to extract these singularities is to split the singular integrands into two terms: one that is regular and can be numerically evaluated (e.g., by a Gaussian quadrature) and another that contains a removable singularity. Four different situations are evaluated in the following way [9]:

1. The source and field segments are far away from each other: all integrals in Eq. (2) are regular and are numerically evaluated (e.g., by Gaussian quadratures).
2. The source and field segments are close to each other and close to the symmetry axis: in this case, numerical evaluation of the α' integral may provide inaccurate results due to the large variation of R in the limit $\varphi \to 0$. So, the integral α' in Eq. (2) is rewritten in a different format and divided in two parts: one that is regular and evaluated by Gaussian quadrature and another that contains a removable singularity and can be integrated analytically. The integrals α and φ are numerically evaluated by Gaussian quadratures.
3. The source and field segments are close to each other and distant from the symmetry axis: in this situation, the φ integral presents inaccuracy in the limit $\varphi \to 0$ due to the large values of ρ and ρ'. The strategy in this case is to subtract from the integral φ in Eq. (2) its approximation, in the limit $\varphi \to 0$, and lead the numerical evaluation. Then, the analytical solution of the limiting approximation is added. The integrals α and α' are numerically evaluated by Gaussian quadratures.
4. The source segment coincides with the field segment: the integral (2) has singularities when $\alpha \to \alpha'$ and $\varphi \to 0$. In this case, a process similar that used in the situation 3 is adopted.

3. NUMERICAL RESULTS

To evaluate the numerical convergence of the adopted singularity extraction, the EFIE, CFIE, and Müller formulations were solved in the analysis of a plane-wave scattering from spherical and cylindrical bodies (Fig. 1). For spheres, the accuracy is verified against analytical solutions based on Mie series using the total RMS error:

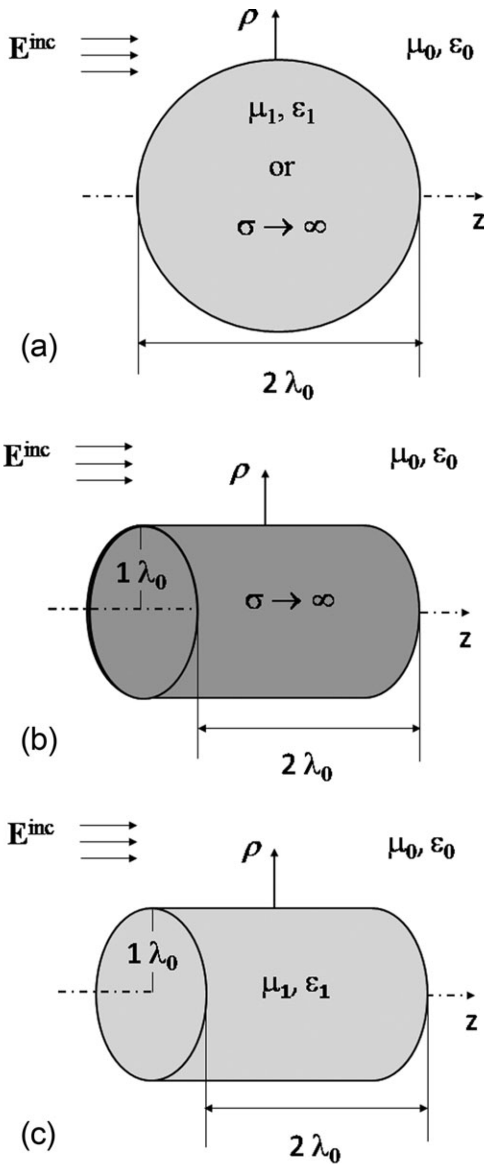

Figure 1 Plane-wave scattering from homogeneous: (a) sphere, (b) conducting cylindrical shell, and (c) dielectric cylinder

$$\text{Error}_{\text{RMS}}(\%) = \left(E_{\text{J}t} + E_{\text{J}\varphi} + E_{\text{M}t} + E_{\text{M}\varphi}\right)/4, \tag{3}$$

with E_X representing a RMS error defined over all X currents:

$$E_X(\%) = \sqrt{\frac{1}{N}\sum_{m=1}^{N}\left(\left|X_m^{\text{MoM}} - X_m^{\text{Mie/CST}}\right| \Big/ \left|X_m^{\text{Mie/CST}}\right|\right)^2}, \tag{4}$$

where X represents an electric (J_{t} or J_ϕ) or magnetic (M_{t} or M_ϕ) surface current component with superscripts ''MoM'' and ''Mie'' denoting the numerical and analytical solutions, respectively. For cylinders, numerical MoM results are compared with those obtained by the CST© software (X^{CST}).

The first case study is a PEC sphere with radius equal to $1\lambda_0$. The analysis was conducted using the CFIE formulation [2]. Different numbers of segments per λ_0 (Seg/λ_0) were used to represent the sphere generatrix and, consequently, the basis and testing functions subdomains. Over each segment, the regular integrals in α and α' of Eq. (2) were both evaluated using a NIP-point Gaussian quadrature, with NIP varied from 1 to 10. Singularities were removed by the extraction technique detailed in Ref. 9. Figures 2(a) and 2(b) show the RMS error as function of NIP with and without the singularity extraction, respectively. When the extraction technique is not used, the integrals are evaluated by Gaussian quadratures, where for coincident source and field segments α' NPI $= \alpha$ NPI $+ 1$ to avoid singularity problems. The RMS error convergence is attained with a two-point Gaussian quadrature when the singularity extraction is applied. Comparing Figures 2(a) and 2(b), it can be observed that the singularity extraction significantly reduces the RMS error, which diminishes when Seg/λ_0 is increased. Figure 2(c) shows the MoM matrix condition number as function of NIP using different numbers of Seg/λ_0 when the extraction technique is used, where one observes that it is not significantly affected by NIP. However, when the extraction technique is not used the MoM matrix condition number decreases as NPI increases as illustrated in Figure 2(d). From Figures 2(c) and 2(d), it can be observed that when the extraction technique is used the MoM matrix condition number decreases.

In this analysis, the surface current distribution has small oscillations, as illustrated in Figure 3(a) (length S is measured along the circular generatrix). So, as Seg/λ_0 increases the MoM matrix condition number also increases, yielding an ill-conditioned linear system, especially when the singularity extraction is not applied, as suggested in Figure 2(d). This behavior can be explained by the magnitude of the elements of a typical MoM

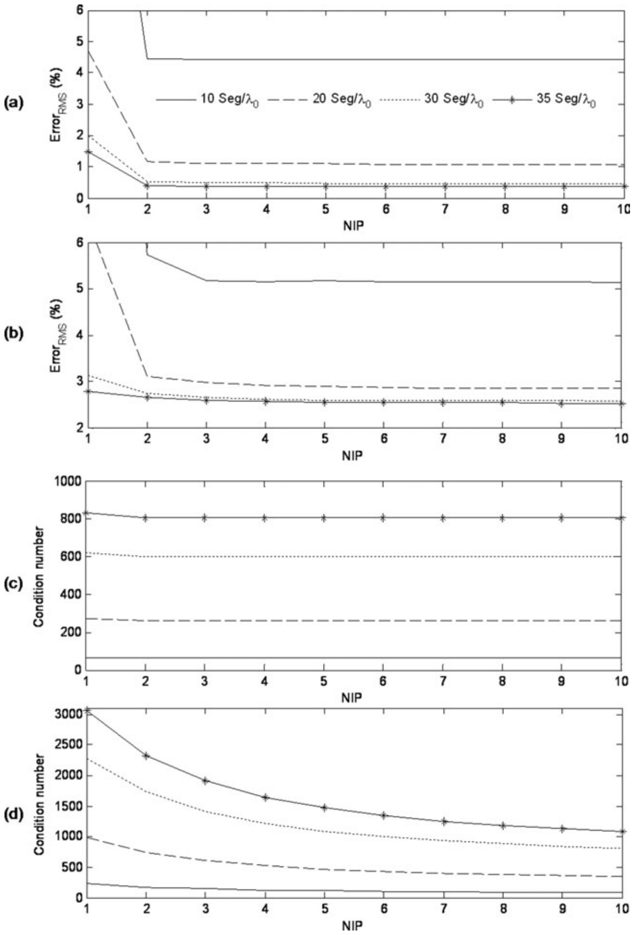

Figure 2 PEC sphere: RMS error (a) with and (b) without singularity extraction and MoM matrix condition number (c) with and (d) without singularity extraction

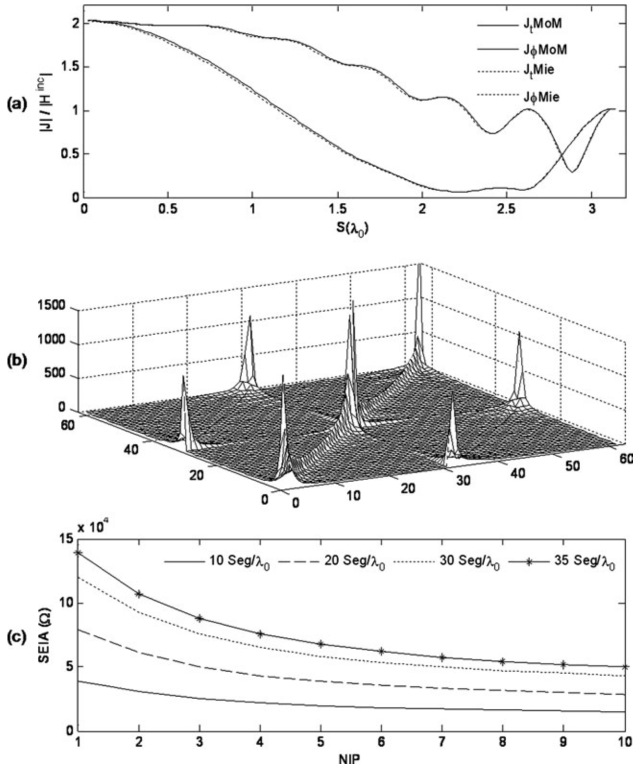

Figure 3 PEC sphere: (a) normalized electric current, (b) MoM matrix elements (NPI = 5 and Seg/λ_0 = 30), and (c) SEIA

matrix, as illustrated in Figure 3(b) for NPI = 5 and Seg/λ_0 = 30. The elements in the main diagonals of the submatrices related to the $\hat{t}$ and $\hat{\phi}$-currents (i.e., elements associated with singular points) have higher amplitudes, particularly those elements corresponding to generatrix segments close to the symmetry axis. This is related to the division by ρ, ρ', or $\rho\rho'$ in Eq. (2). In these cases, the integrals in α and α' are evaluated using a singularity extraction technique or using more points in Gaussian quadratures. When the extraction technique is not used, the absolute values of these elements decrease as NIP increases, as shown in Figure 3(c) with sum of the elements that intercept the symmetry axis (SEIA) being the sum of absolute values of the elements in the main diagonals of the MoM matrix corresponding to segments that intercept the symmetry axis. As the absolute values of these elements diminish, the MoM matrix becomes better conditioned. SEIA increases with Seg/λ_0 as the singularities become more severe. It is important to observe that when singularity extraction is applied, the RMS error and the MoM matrix condition number improve and converge is achieved for NIP = 2, independently from Seg/$\lambda_{0.}$

In the next case study, the plane-wave scattering from a dielectric sphere with radius equal to $1\lambda_0$ and relative permittivity $\varepsilon_r = 5$ was analyzed by Müller formulation [3]. From Figure 4(a), one observes that when singularity extraction is applied, the RMS error does not vary significantly for NIP $\geq$ 2, but it does diminish significantly when Seg/λ_0 is increased. When singularity extraction is not applied, convergence is attained only for large NIP values and small Seg/λ_0 values [Fig. 4(b)]. This behavior is more evident for larger dielectric constants, as illustrated in Figure 5 for $\varepsilon_r = 20$. As in the first case study, the singularity extraction reduces the MoM matrix condition number, which does not vary significantly for NIP $\geq$ 2 [Figs. 4(c) and 4(d)]. For the dielectric sphere with $\varepsilon_r = 5$, the electric and magnetic current distributions have a significant oscillatory behavior, as illustrated in Figures 6(a) and 6(b). So, when Seg/λ_0 increases, the linear system does not become so ill-conditioned (the matrix determinant is not very small compared to the matrix elements), as in the conducting sphere case. Then, for this dielectric sphere, as Seg/λ_0 increases the increase of the MoM matrix condition number is less significant.

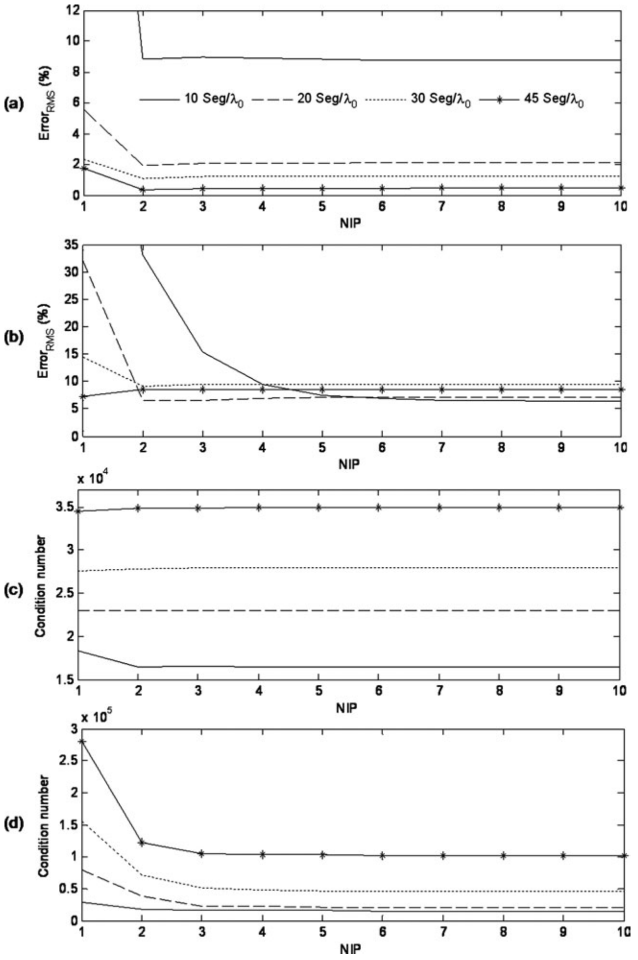

Figure 4 Dielectric sphere with ε_r = 5: RMS error (a) with and (b) without singularity extraction and MoM matrix condition number (c) with and (d) without singularity extraction

The third case study is the plane-wave scattering from a cylindrical shell as depicted in Figure 1(b). The analysis was conducted using EFIE. The results presented in Figures 7(a)–7(d) indicate that the current RMS error and the MoM matrix condition number have different values, but about the same behavior with respect to NIP and Seg/λ_0 already observed for the

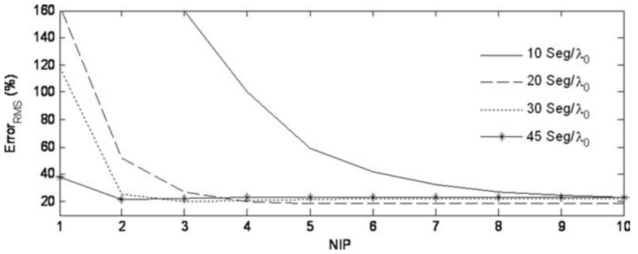

Figure 5 RMS error without singularity extraction for a dielectric sphere with $\varepsilon_r = 20$

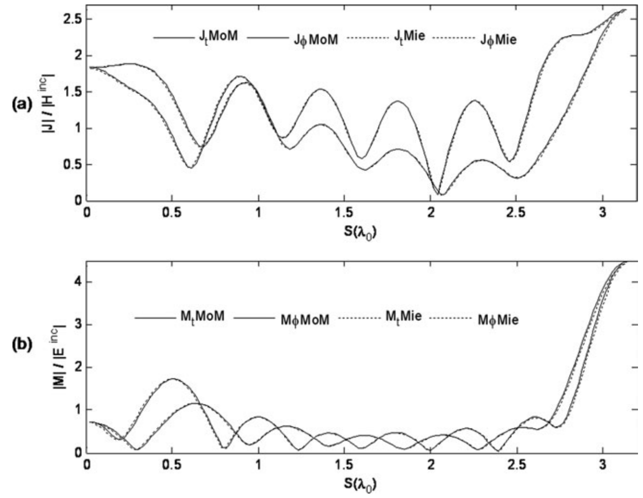

Figure 6 Dielectric sphere with $\varepsilon_r = 5$: normalized (a) electric and (b) magnetic currents

conducting sphere (Fig. 2). However, in this case, no segments intercept the symmetry axis, as the cylinder is an open shell. So, the integrals with division by ρ, ρ', or $\rho\rho'$ in Eq. (2) do not lead to elements in the MoM matrix, corresponding to generatrix segments close to the symmetry axis, so larger. Then, when extraction is not used and NIP increases these integral are not considerably improved and, consequently, the MoM matrix condition number is not significantly modified. The equivalent surface currents obtained in this case study (NPI = 2 and Seg/λ_0 = 30) are illustrated in Figure 8 together results obtained by CST$^©$ software, and one observes a good concordance between both results.

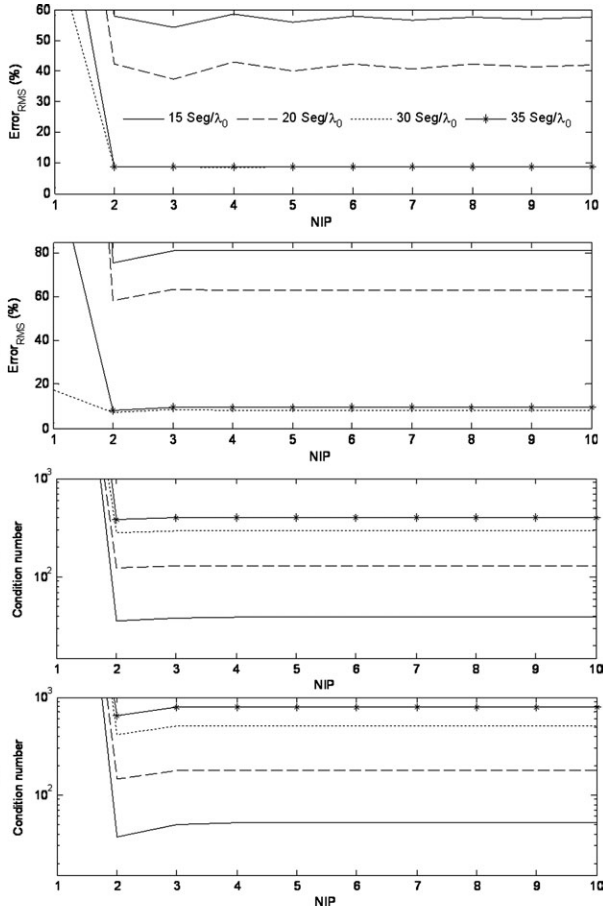

Figure 7 PEC cylinder: RMS error (a) with and (b) without singularity extraction and MoM matrix condition number (c) with and (d) without singularity extraction

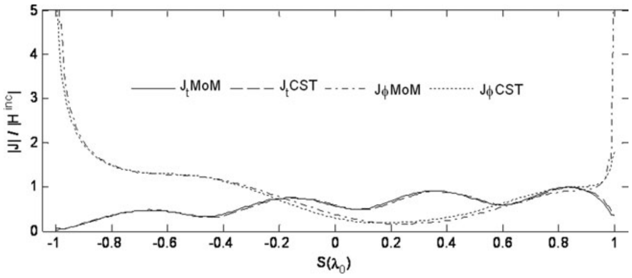

Figure 8 PEC cylinder: normalized electric current

The last case investigated is the plane-wave scattering from a dielectric cylinder with $\varepsilon_r = 2$, as illustrated in Figure 1(c). The analysis was conducted using Müller formulation [3]. The RMS error and MoM matrix condition number are shown in Figure 9. The equivalent surface currents are illustrated in Figures 10(a) and 10(b) together with results obtained by the CST$^©$ software.

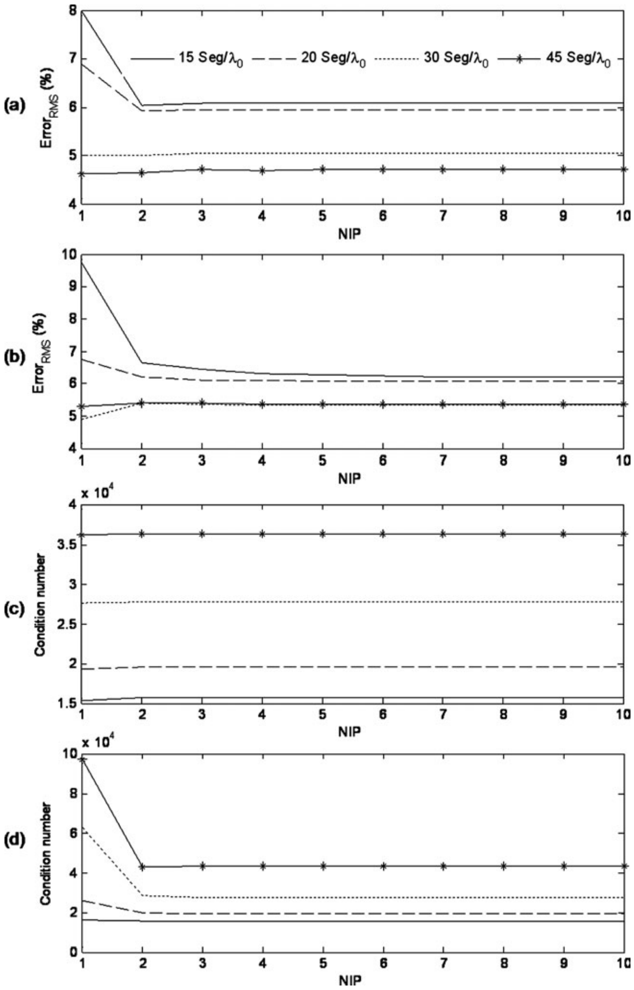

Figure 9 Dielectric cylinder with $\varepsilon_r = 2$: RMS error (a) with and (b) without singularity extraction and MoM matrix condition number (c) with and (d) without singularity extraction

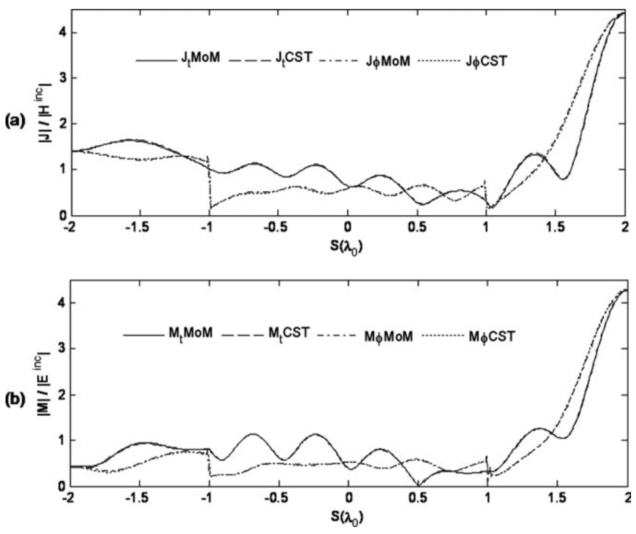

Figure 10 Dielectric cylinder with $\varepsilon_r = 2$: normalized (a) electric and (b) magnetic currents

In this case, the current RMS error and the MoM matrix condition number vary with respect to NIP and Seg/λ_0 as in the case of the dielectric sphere with $\varepsilon_r = 5$ (Fig. 4), except that the convergence is achieved for smaller NPI values when the extraction technique is not used.

4. CONCLUSIONS

In this work, the convergence of the MoM solution using a particular singularity extraction was investigated in the plane-wave scattering from dielectric and conducting spheres and cylinders. Results indicate that when singularity extraction is applied, convergence is attained with a two-point Gaussian quadrature (NIP = 2) over the segments used to describe the BOR generatrix and, consequently, the equivalent current distributions. The number of segments per wavelength influences the RMS error of the equivalent currents, which diminishes when more segments are used. When singularities are not carefully removed, convergence is attained only for larger NIP values, particularly for dielectric BORs with large dielectric constants. The singularity extraction reduces the MoM matrix condition number, which is affected by the number of segments used to describe the BOR generatrix. This influence depends on the behavior of the surface current distribution, that is, for current distributions with small oscillations, the MoM matrix condition number increases significantly when more segments are used to represent the BOR generatrix and for current distributions with highly oscillatory behavior this increase is smaller.

ACKNOWLEDGMENTS

This work was partially supported by FAPEMIG APQ-01073-08, CAPES RH-TVD 254/2008 and CNPq.

REFERENCES

1. J. Mautz and R. Harrington, An improved E-Field solution for a conducting body of revolution, Tech. Report TR-80-1, Dept. Electrical and Computer Engineering, Syracuse University, 1980.
2. J. Mautz and R. Harrington, H-field, E-field and combined field solutions for bodies of revolution, IEEE Trans Antennas Propag 27 (1979), 157–164.
3. A.A. Kishk and L. Shafai, Different formulations for numerical solution of single or multibodies of revolution with mixed boundary conditions, IEEE Trans Antennas Propag AP-34 (1986), 666–673.
4. U.C. Resende, F.J.S. Moreira, and O.M. Pereira Filho, EMFIE and MEFIE formulations for the analysis of scattering from dielectric and composite bodies of revolution, Microwave Opt Technol Lett 53 (2011), 398–402.
5. S.D. Gedney and R. Mittra, The use of the FFT for the efficient solution of the problem of electromagnetic scattering by a body of revolution, IEEE Trans Antennas Propag 38 (1990), 313–322.
6. D.H. Werner, An exact integration procedure for vector potentials of thin circular loop antennas, IEEE Trans Antennas Propag 44 (1996), 157–165.
7. D.H. Werner, A method of moments approach for the efficient and accurate modeling of moderately thick cylindrical wire antennas, IEEE Trans Antennas Propag 46 (1998), 373–382.
8. A.W. Glisson, On the development of numerical techniques for treating arbitrarily-shaped surfaces, Ph.D. dissertation, Univ. Mississippi, 1978.
9. U.C. Resende, F.J.S. Moreira, and O.M. Pereira Filho, Efficient evaluation of singular integral equations in moment method analysis of bodies of revolution, J Microwaves Optoelectron 6 (2007), 373–391.
10. U.C. Resende and F.J.S. Moreira, Numerical convergence of method of moments in the analysis of bodies of revolution, 17th International Conference on the Computation of Electromagnetic Fields (COMPUMAG 2009), Florianopolis, Brazil, pp. 817–818, November 2009.
11. A. Kishk and L. Shafai, Improvement of the numerical solution of dielectric bodies with high permittivity, IEEE Trans Antennas Propag 37 (1989), 1486–1490.

STUB-LOADED BENT MONOPOLE ANTENNA WITH INDEPENDENT FREQUENCY TUNING CAPABILITY FOR COMPACT WIRELESS USB DONGLES

Seong Jae Jeong and Keum Cheol Hwang
Division of Electronics and Electrical Engineering, Dongguk
University-Seoul, 26, Pil-dong 3-ga, Chung-gu, Seoul 100-715
South Korea; Corresponding author: kchwang@dongguk.edu

Received 31 January 2012

ABSTRACT: *In this article, compact monopole antenna with independent resonant frequency tuning capability is proposed. The antenna radiating patch consists of a simple, bent monopole element and an open stub. The bent monopole acts as a main radiator in 2.5 GHz band, whereas the open stub serves in 5.5 GHz band. A prototype of the proposed antenna was fabricated, and the reflection and radiation characteristics were measured to validate the antenna performances. Measured impedance bandwidths (VSWR < 2) exhibits dual-broadband resonances, which are 2.08–3.02 GHz (lower band) and 5.13–6.15 GHz (upper band), corresponding to 36.9 and 18.1%, respectively. Therefore, VSWR bandwidth of the proposed design covers not only the WiBro, WiMAX, Bluetooth, 2.4 GHz WLAN, S-DMB, but also the 5.2/5.8 GHz WLAN services. The peak gain was 5.76 dBi.* © 2012 Wiley Periodicals, Inc. Microwave Opt Technol Lett 54:2548–2552, 2012; View this article online at wileyonlinelibrary.com. DOI 10.1002/mop.27159

Key words: *wireless USB dongle; bent monopole; open stub; dual-band antenna*

1. INTRODUCTION

With the rapid development of wireless communication systems, multiband antenna has become one of the most important issues and attracted much interest. Most of modern portable devices require a miniaturized multiresonant antenna to cover various